Engineering Structures 195 (2019) 324–339

Contents lists available at ScienceDirect

Engineering Structures

journal homepage: www.elsevier.com/locate/engstruct

Seismic reliability assessment of code-conforming reinforced concrete buildings made with electric arc furnace slag aggregates

Flora Faleschini[a,b], Mariano Angelo Zanini[a,*], Klajdi Toska[a]

[a] Dept. of Civil, Environmental and Architectural Engineering, University of Padua, Via Marzolo 9, 35131 Padua, Italy
[b] Dept. of Industrial Engineering, University of Padua, Via Gradenigo 6, 35131 Padua, Italy

ARTICLE INFO

Keywords:
EAF slag
Reinforced concrete moment frames
Seismic fragility
Seismic reliability

ABSTRACT

Recent studies have demonstrated how Electric Arc Furnace (EAF) concrete represents a sustainable alternative to ordinary concretes, and that it could be satisfactorily employed to realize reinforced concrete (RC) elements. However, a comprehensive study about the effects of its use in RC structural systems, both in terms of structural safety under static and dynamic loads, and environmental impacts along the whole life cycle, has not been investigated yet. This work analyzes the seismic reliability of standard residential buildings (cast in place RC frames), considering three different configurations (3-, 6- and 9- story building type) designed considering ordinary concretes made with natural aggregates (NA) according to the novel Italian seismic code, which is similar to the Eurocode 8 approach. Non-linear time history analyses have been carried out to investigate the seismic response of the analyzed cases comparing results obtained from the benchmark structures (i.e. the NA ones) with those coming from the same made with EAF mixes, in order to verify the suitability in using sustainable EAF concrete mixes in seismic areas. Lastly, a seismic reliability analysis has been carried out for comparative purposes, demonstrating how EAF concrete overstrength compensates for the extra efforts that the analyzed RC frames may undergo during seismic events.

1. Introduction

Among the Sustainable Development Goals (SDG) that have been adopted by the Agenda 2030 of the United Nations [1], one of the main global challenges that the construction market has to face, together with the society, is to substantially reduce waste generation through prevention, reduction, recycling and reuse policies. In this field, the reduction of waste disposal through the promotion of recycling opportunities as construction materials has been largely a matter of study and research within the scientific world. Specifically, an extensive research has been devoted to safely use various type of waste in the construction industry, and due to the great amount of natural aggregates (NAs) consumption, this represents an important part of the market that has been explored. As indicative numbers, the European aggregates demand alone is 2.7 billion tonnes per year [2]; additionally, also for structural concrete production it is worth recalling that aggregates represent 70% in volume of a concrete mixture, in average.

The most well-known case of recycling is that of Construction and Demolition Waste (C&DW), which can be used to produce Recycled Aggregates (RAs); their use is currently allowed and regulated in most of the building codes and standards around the world [3–5]. More recently, the suitability of using other kind of waste and by-products to produce so-called industrial aggregates has been object of a dynamic research, which for instance analyzed the applicability of plastic waste [6,7], recycled waste glass [8,9], recycled tires [10,11], and many other by-products, particularly from steelmaking industry [12–15]. Among this last class of by-products, electric arc furnace (EAF) slag has displayed excellent properties when used as coarse aggregate in concrete, both in terms of mechanical strength [16–20] and durability [21–23], that make it a good candidate for large scale use in structural concrete. Its use has been demonstrated suitable also to cast self-compacting mixtures [24,25], even though poorer workability of fresh EAF concrete has been recorded in many works, due to the angular shape of its particles. Particularly, concrete compressive strength, tensile strength and elastic properties are enhanced if compared to ordinary concrete mixtures, although a higher specific weight is reported, due to presence of iron and other heavy-weight metals in the composition of the slag.

First experimental evidences on the behavior of reinforced concrete (RC) elements with EAF slag as coarse recycled aggregate have demonstrated an improved flexural and shear capacity in RC beams subject to monotonic loading under four point bending test [26,27].

* Corresponding author.
E-mail address: marianoangelo.zanini@dicea.unipd.it (M.A. Zanini).

https://doi.org/10.1016/j.engstruct.2019.05.083
Received 8 March 2019; Received in revised form 23 May 2019; Accepted 27 May 2019
Available online 11 June 2019

Concerning bond between steel and EAF concrete, local bond strength-slip curves demonstrates at least similar or even improved ultimate and frictional bond strength compared to conventional concretes [28]. Ductility of RC columns tested under uniaxial compression is at least similar to that of ordinary mixtures [29], and the shear strength of exterior RC beam-column joint is improved [30]. When subject to cyclic lateral loading, i.e. under seismic-like action, EAF concrete joints displayed superior behavior also in terms of ductility, dissipated energy, reduced cracking patter, and similar stiffness decay than the reference joint made with ordinary concrete. This evidence was obtained not only for the joint casted with the same mix design, changing only the type of aggregates, but also for a joint realized with less cement dosage, and hence, a significantly reduced environmental footprint [30]. Other configurations were also numerically investigated, e.g. changing the column axial load or the amount of reinforcement (transvers and longitudinal) in the beam and in the column, thus analyzing both the situations of strong beam – weak column and strong column – weak beam [31].

The above literature has evidenced that EAF slag concrete can be suitably applied in gravity structures, where its heavy-weight (estimated in about + 15% increase) and high strength result as positive features: as illustrative example, different applications can be found in structures that requires shielding for radioprotection [32]. However, doubts might arise about its efficacy when applied in elevation RC structures, because the enhanced mechanical strength might not sufficiently balance the increased dead loads of the RC EAF concrete elements. In particular, in seismic design context, an increase of self-weight can impact vibration modes and related fundamental periods, thus resulting in a variation of seismic forces along the structural members, and this can worsen the seismic response of stiff buildings (i.e. those with a limited number of floors). Accordingly, this paper aims to solve this question, analyzing three classes of EAF concrete, characterized by increasing aggregates replacement ratio, used as replacement mixes in the construction of code-conforming earthquake-resistant RC frame buildings built with ordinary concretes made with NAs.

For such purpose, a wide dataset of experimental tests on EAF concrete specimens collected in scientific literature is build-up, based on two previous versions of some of the authors [33,34]. Data were statistically processed in order to extract the ratios of variation in main mechanical concrete parameters (i.e. compressive and tensile strength, and elastic moduli) and in self-weight loads for three different EAF concrete classes, namely C1, C2 and A with respect to the benchmark concrete mixes made with NAs. Hence, three different geometrical configurations of regular earthquake-resistant RC frame buildings with three, six and nine stories, respectively, have been designed according to the current Italian Codes for Constructions (NTC2018 [5]) for a medium-to-high seismic hazard site. A set of non-linear time history analyses (NLTHAs) has been then run in order to investigate the seismic behavior of the analyzed structural system and to further derive seismic fragility functions. Hence, a seismic reliability assessment has been carried out on the whole combination of the investigated structural configurations and concrete mixes, for an overall of 12 combinations (i.e., four material types and three geometrical configurations), thus investigating the variation of structural safety margins related to the use of the sustainable EAF concretes in replacement to a classic NA concrete mix.

2. EAF slag and its use as aggregate in structural concrete

2.1. EAF slag

EAF slag is a by-product of steelmaking production, being the result of the addition of fluxes (e.g., lime) and oxygen injection inside the electric arc furnace, to remove the impurities from the molten steel bath. After cooling, from temperatures up to 1300 °C to ambient conditions, EAF slag becomes a solid, dark-grey stony material, which characteristics depend on several factors, such as the type of steel to be produced (e.g., carbon or stainless steel), scrap composition, slag cooling method and speed, and further weathering process.

Table 1
Physical properties of EAF slag compared to dolomitic aggregate (NA).

	Apparent density (kg/m^3)	Water absorption (%)	Porosity (%)	Shape
EAF 0–4 mm	3800	1.0–1.5	2.0	Crushed
EAF 4–16 mm	3950	< 1.0	0.5–2.7	Crushed
NA 0–4 mm	2760	–1.5	< 2.0	Roundish
NA 4–16 mm	2790	< 0.5	0.9–1.8	Roundish

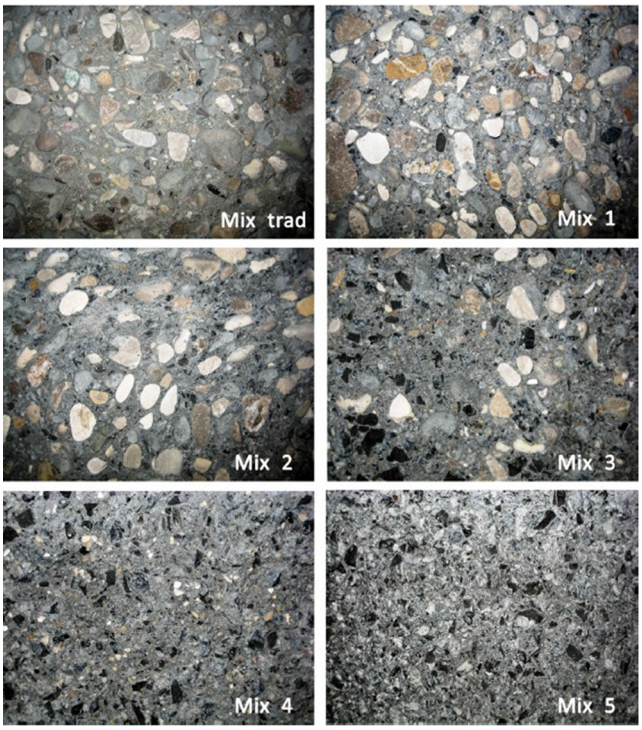

Fig. 1. Splitting surface of EAF concretes realized with increasing content of slag (from left top 0% slag, to right bottom 100% slag); retrieved from the experimental campaign reported in [22].

Table 2
Concrete classes considered for the analysis: range of variability.

	Reference	Class EAF-C1	Class EAF-C2	Class EAF-A
w/c ratio	0.35–0.70	0.40–0.50	0.51–0.67	0.35–0.70
EAF [type]	–	> 4 mm	> 4 mm	all
ρ_c [kg/m^3]	2260–2510	2630–3001	2380–3045	2500–3180
f_c [MPa]	22.0–65.0	31.6–70.3	20.3–55.7	25.1–77.9
f_{ct} [MPa]	2.20–5.21	3.45–5.65	1.80–4.38	3.56–5.89
E_c [GPa]	24.0–42.7	42.2–49.5	23.6–40.5	37.4–48.3

Table 3
Ratios between EAF and Reference concrete properties.

	Class EAF-C1	Class EAF-C2	Class EAF-A
$\rho_{c,EAF}/\rho_{c,Ref}$	1.166	1.166	1.154
$f_{c,EAF}/f_{c,Ref}$	1.395	1.404	0.915
$f_{ct,EAF}/f_{ct,Ref}$	1.280	1.100	1.080
$E_{c,EAF}/E_{c,Ref}$	1.330	1.100	1.040

Table 4
Properties of C25/30 concrete made with the analyzed concretes.

	Reference	Class EAF-C1	Class EAF-C2	Class EAF-A
ρ_c [kg/m^3]	2400	2798	2799	2769
f_c [MPa]	33.0	46.0	46.3	30.2
f_{ct} [MPa]	3.30	4.22	3.63	3.56
E_c [GPa]	27.0	35.9	29.7	28.1

Particularly, EAF slag from carbon steel production is mainly composed of iron, calcium, silicon and aluminum oxides, plus minor concentrations of manganese and magnesium [35]. Also, other metals may be present in trace concentrations. For a more detailed characterization, readers can find a detail analysis of slag physic-chemical properties, morphology and mineralogy in [35]. Typically, EAF slag requires to be pre-treated before its potential use as aggregate for concrete production, due to the presence of certain amount of free lime and free magnesium oxide, that might induce swelling phenomena, and hence, volumetric instability of the matrix where it will be employed. To reduce the impact of such phenomenon, a weathering protocol is adopted by most of the companies that manage the slag, with significant improvements in terms of slag expansion reduction [35]. It consists in at least three months of outdoor exposure, followed by crushing/deferrization/treatment operations to obtain the required aggregates grading, and lastly a further week of daily wetting/drying cycles, that aims to remove the superficial free CaO and allows the leaching of heavy metals. EAF slag is characterized by high density, relatively low porosity (higher for the fine fraction) and high crushing resistance. Typical Los Angeles values are less than 20%. Table 1 summarizes the main physical properties of the slag for two size fractions, compared to a reference dolomitic aggregate, very common in North-East Italy. Apparent density and water absorption are evaluated with the picnometer method, whereas Mercury Intrusion Porosimetry (MIP) tests were carried out to establish aggregates porosity.

2.2. EAF concrete: Fresh and hardened concrete properties

When EAF slag is used to replace NA in cement-based materials, generally it has a positive influence on mechanical properties, such as compressive and tensile strength. However, such effect strongly depends on the type and amount of the substitution; indeed, it has been experimentally demonstrated that when coarse aggregates are used, they have a beneficial impact, whereas, when also the fine fraction is employed, such properties enhancement is more limited [22]. Concerning fresh properties, it is worth to recall that the use of EAF slag generally worsen the workability of the mixtures, and this is particularly true when natural sand is replaced at high substitution ratio, due to higher water absorption and porosity than NA. Also the crushed shape of slag negatively affects the fresh behavior of EAF concrete; however, the use of water reducing admixtures (WRA) ensures reaching high flowability and pumpability. EAF slag impacts significantly on the fresh and hardened concrete specific weight: depending on the slag composition, and specifically on the amount of iron and heavy weight oxides, it might increase this property up to 15–20%. Such variation is almost the same regardless of the size fraction used. Instead, concrete compressive strength is affected depending on several factors, i.e. the

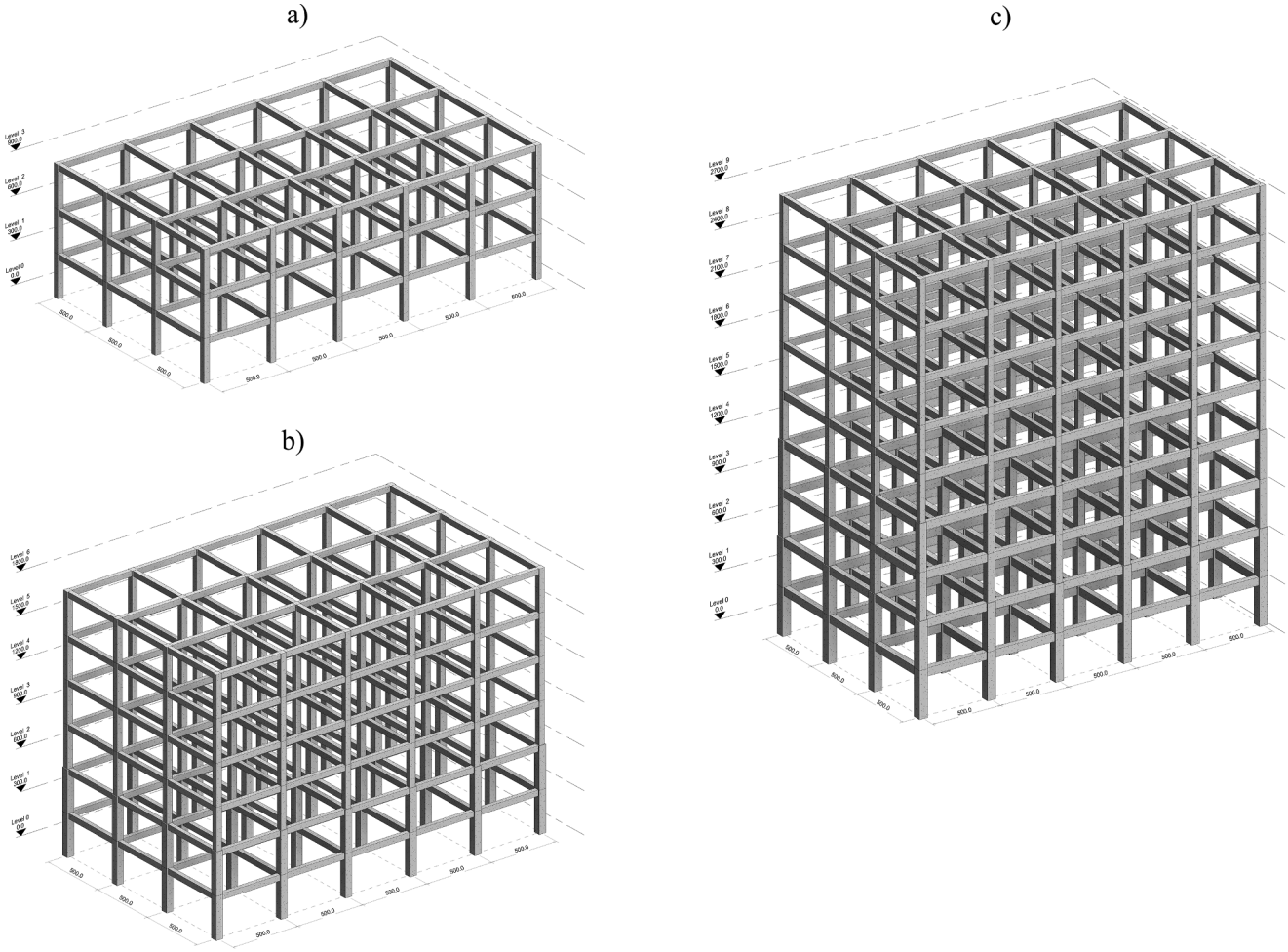

Fig. 2. RC frame layouts analyzed: 3- (a), 6- (b) and 9-story (c) building archetypes.

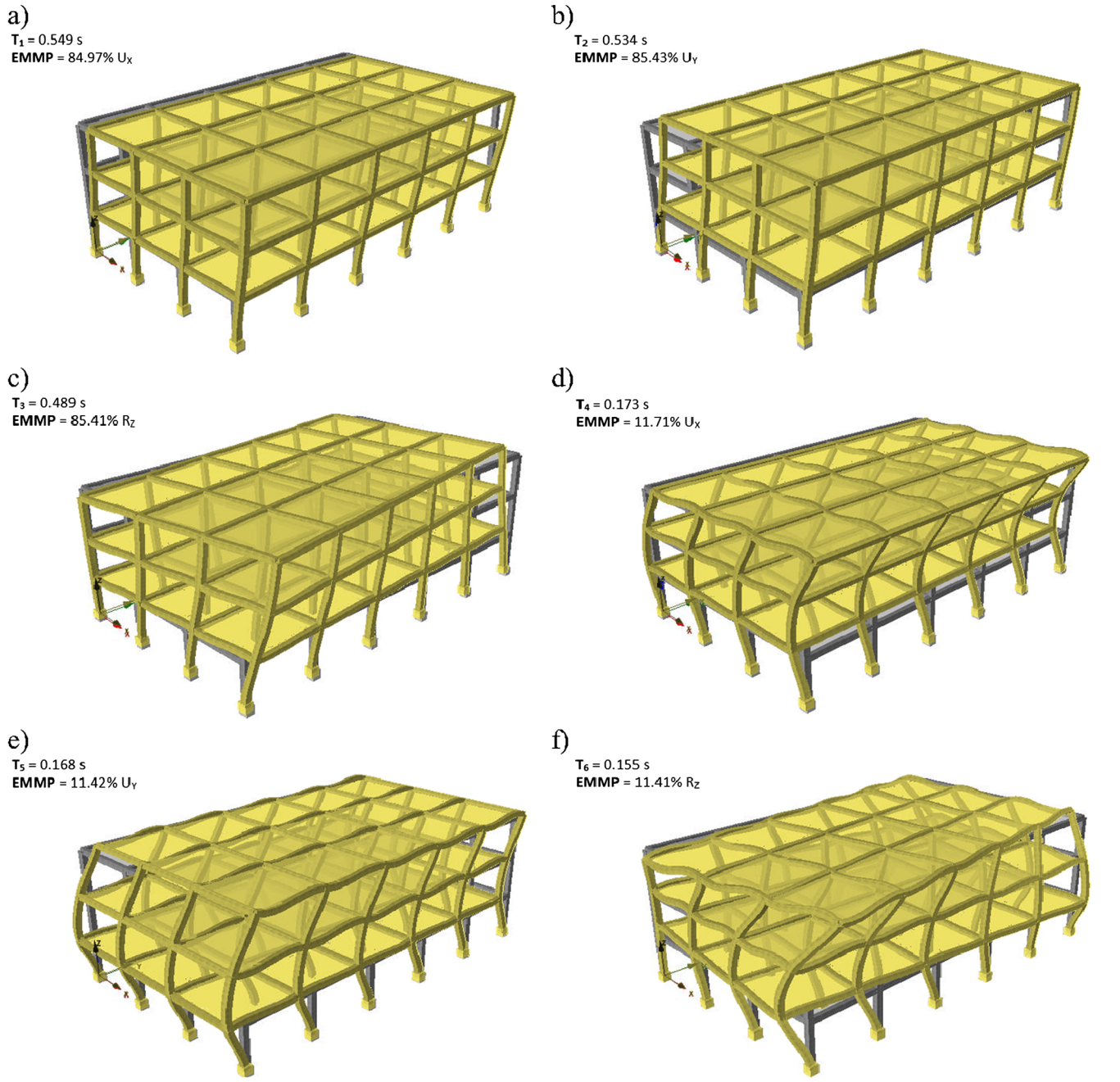

Fig. 3. Main vibration modes for the 3-story RC frame archetype.

size fraction of the slag (coarse and/or fine), the amount of the substitution (e.g., [22] recommend maintaining at least 50% of natural sand to do not experience high strength losses), and the quality of the matrix where the slag is employed. For this latter variable, some of the authors already observed that the highest strength improvement was displayed in concretes with a good quality of the cementitious matrix, because the slag can better exploit its strength and bond with the matrix, rather than in concretes with a high water/cement (w/c) ratio [28]. Such strength enhancement has been also explained due to the high quality of the interfacial transition zone (ITZ) between slag and cementitious matrix [17], which has a low thickness due to the enrichment at slag surface in calcite [35], that promotes the bond and hence the cohesiveness of the concrete. The same trend is observed in literature about the influence of slag on tensile strength. Concerning elastic properties, it is worth recalling that they are mainly influenced by aggregates type, and specifically by their elastic modulus. For this reason, a general improvement of elastic modulus in EAF concrete is displayed, regardless of the aggregates size; however, when employed in low-strength matrix, such improvements are more limited. Fig. 1 shows the splitting surface of EAF concretes realized with increasing amount of slag as substitution of both coarse and fine NAs.

2.3. EAF concrete: Impact on specific weight, compressive and tensile strength, elastic modulus

Based on the above context, one of the authors has gathered an experimental dataset which collects 172 samples of concretes [34] from different experimental studies, based on the previous database published in [33]. There, three classes of EAF concretes (other than a reference class) have been distinguished. The samples included in the dataset cover a large range of characteristics: for instance, w/c ranges from 0.35 to 0.7, replacement ratio between 0 and 100%, and the slag

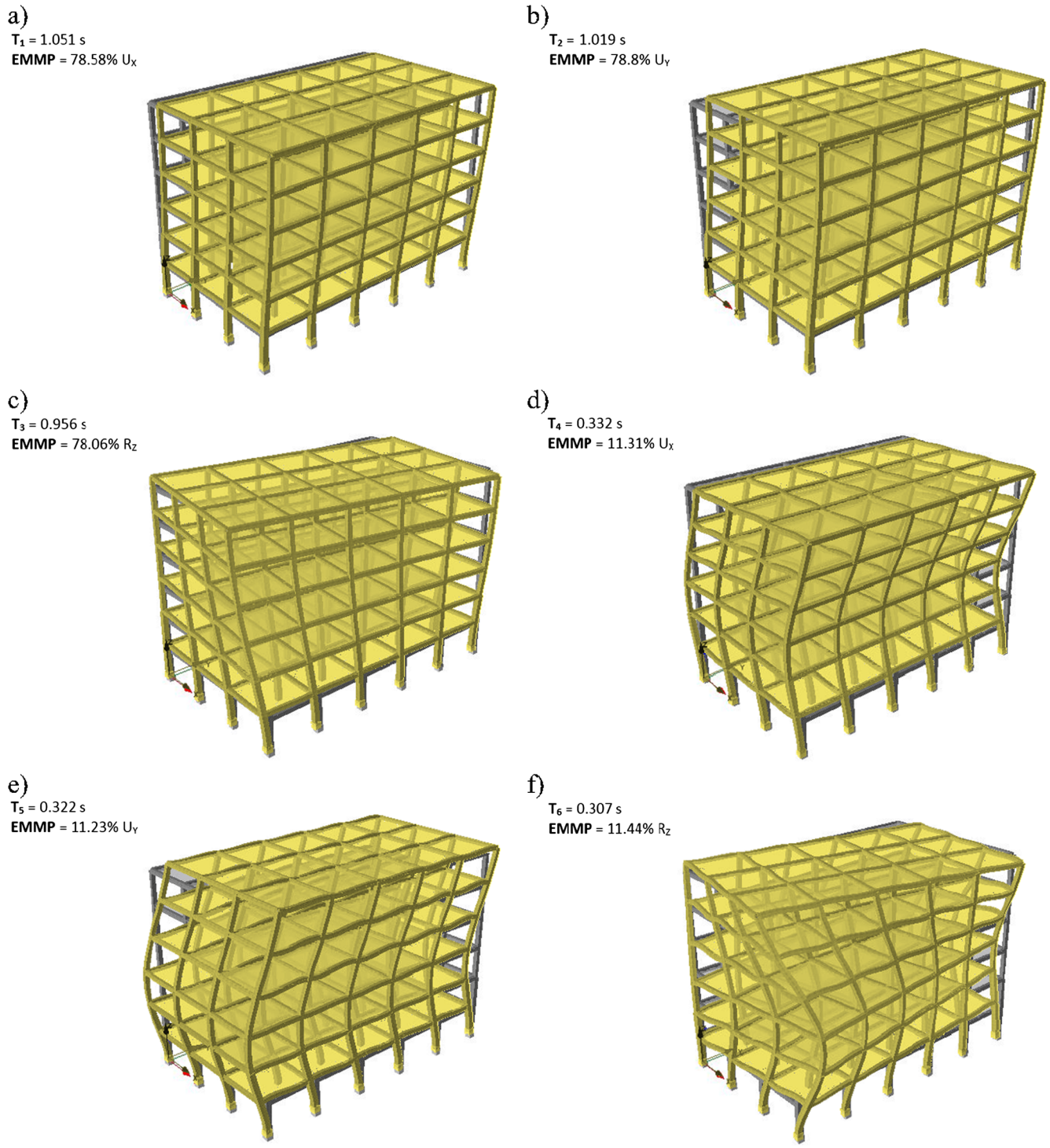

Fig. 4. Main vibration modes for the 6-story RC frame archetype.

grading can be both coarse, fine or all-in. The experimental specific weight of the concretes varies between 2260 kg/m^3 and 3180 kg/m^3, concrete compressive strength between 17 and 78 MPa, tensile strength between 1.8 and 5.9 MPa and, lastly, elastic modulus between 23.6 and 49.5 GPa. Table 2 summarizes the features of each class of concrete, establishing also the range of validity of the relations that have been further developed. The complete dataset can be found in [34], and it is available contacting the authors.

Hence, for each EAF concrete class it was possible to derive a multiplying factor that correlates the analyzed property with that of the reference concrete within each experimental campaign included in the dataset, and overall, results of this analysis are reported in Table 3. There, ratios of $\rho_{c,EAF} / \rho_{c,Ref}$, $f_{c,EAF} / f_{c,Ref}$, $f_{ct,EAF} / f_{ct,Ref}$, and $E_{c,EAF} / E_{c,Ref}$ are presented for the three class of EAF concretes analyzed. As an indicative example, Table 4 reports also the property for C25/30 strength class concrete (as defined in [5]), in case of being realized with the three classes of EAF concrete. Such result has been also used in the next steps of the work to characterize the constitutive behavior of concrete in compression and tension, necessary for the development of the numerical models and execution of seismic reliability analyses.

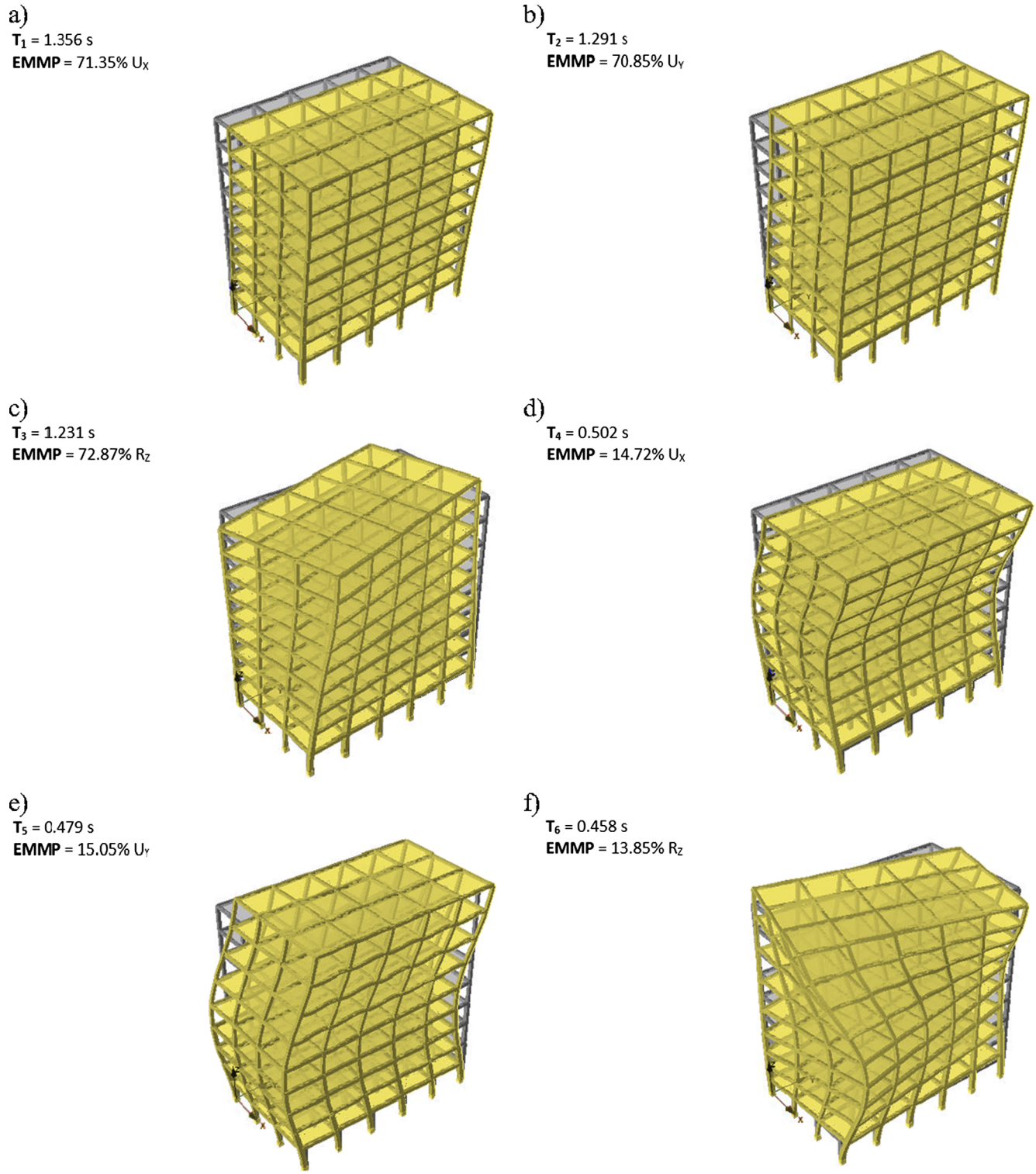

Fig. 5. Main vibration modes for the 9-story RC frame archetype.

3. RC frame code-conforming analyzed case studies

As reported above, replacing natural aggregates with EAF slag impacts on material strength but also on its weight. The higher is the mass, the higher is the seismic solicitation to the structure. To analyze the different structural response due to seismic excitation, three moment frame RC structures were considered with 3-, 6- and 9- stories, respectively. Fig. 2 shows main geometrical features of the investigated RC frames, each characterized by a rectangular plan of 25 m length and 15 m width, with a spacing between consecutive bays equal to 5 m.

A reinforced concrete slab of 20 cm thickness supports a 5 cm layer of screed (0.95 kN/m^2), flooring (0.4kN/m^2) and partition walls (1.6 kN/m^2) as permanent non-structural loads for intermediate floor slabs, whereas no partition walls were considered for the roof slab. The structures are considered for residential intended use, so with an accidental load equal to 2 kN/m^2. As regards seismic actions, they were supposed to be located in a moderate-to-high seismic hazard site, in the Municipality of Pordenone, Northeast Italy, thus deriving from the

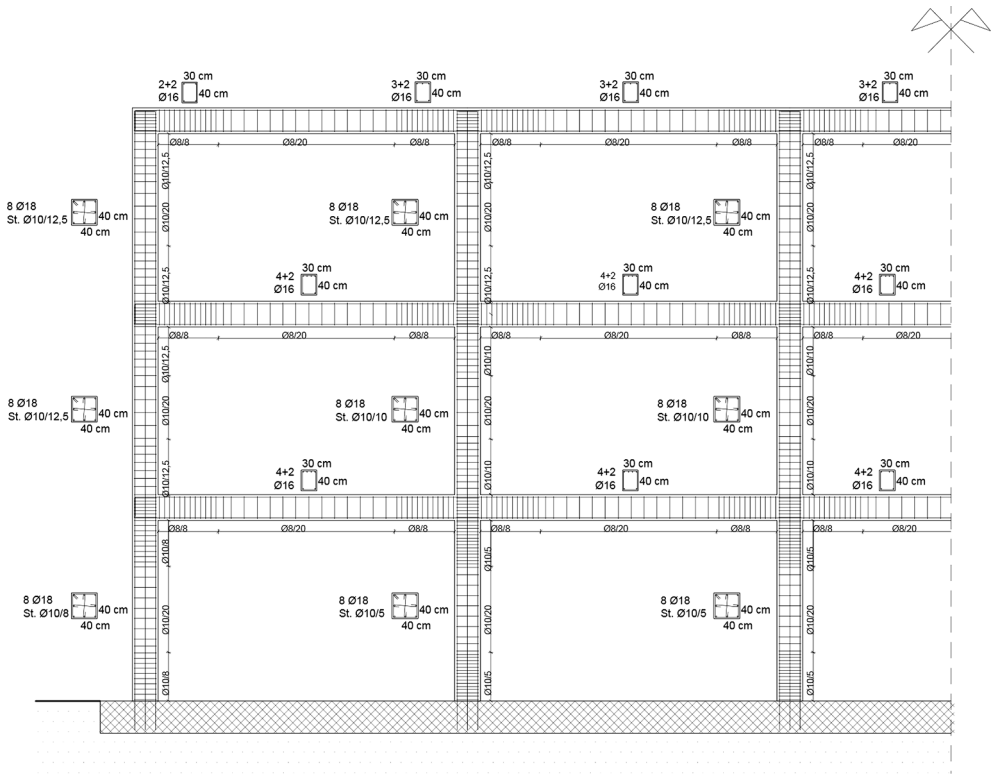

Fig. 6. 3-story RC frame archetype: reinforcement arrangement.

national hazard map the 475-year Uniform Hazard Spectrum parameters (a_g = 0.195, F_0 = 2.441, T_c^* = 0.333) for a soil-B type and a unitary topographic coefficient. Each case-study was thus designed in accordance with the Italian Building Code (NTC18 [5]) considering a low ductility class (Class B), by using a dynamic linear analysis method for computing seismic design loads on structural members, and considering a structure behavior factor q equal to 3.9. Figs. 3–5 illustrate the main vibration modes and related effective modal mass percentage (EMMP) values for each of the analyzed structural systems, showing similar fundamental periods in longitudinal (X) and transversal (Y) directions, equal to about 0.54 s for the 3-story, 1.03 s for the 6-story and 1.32 s for the 9-story archetypes.

Based on the seismic design loads derived from dynamic linear analyses, beam and column members were sized accordingly, using for concrete the Reference C25/30 strength class: Figs. 6–8 illustrates in detail steel reinforcing bars arrangements designed for each of the three analyzed case studies.

4. Theoretical background on seismic reliability analysis

In the context of the Performance-Based Earthquake Engineering (PBEE) framework [36], the occurrence of main earthquakes at the construction site is assumed to be a Homogenous Poisson Process (HPP). Under this hypothesis, and not considering damage accumulation on structures, the process of events causing the structural failure is also represented by an HPP, whose unique parameter, the failure rate λ_f, can be used for computing the failure probability in any time interval. The failure rate λ_f represents therefore one of the most used reliability indicators, mainly due to its simplicity and its unique dependence on the seismic hazard and on the structural behavior. Particularly, it depends on the *hazard curve* λ_{im}, representing the seismicity on a specific site, and on *fragility curve* $P[f|im]$, being the probabilistic structural behavior of a specific structure. The failure rate λ_f is thus computed by applying the Total Probability Theorem, in the following way:

$$\lambda_f = \int_{im} P[f|im] \cdot |d\lambda_{im}| \tag{1}$$

4.1. Seismic hazard estimation

Current state-of-the-art approaches for the computation of λ_{im} are based on the so-called Probabilistic Seismic Hazard Analysis (PSHA, [37–38]) which associates to each im value, the corresponding annual rate of events exceeding it at the site where the structure is located. This calculation involves the three main components that contribute to define the seismicity of a specific area, that are the earthquake occurrence model, the spatial seismogenic model and the ground motion attenuation model. From λ_{im}, $|d\lambda_{\mathrm{im}}|$ is easily obtained as:

$$|d\lambda_{\mathrm{im}}| = -\frac{d\lambda_{\mathrm{im}}}{d(im)} d(im) \tag{2}$$

representing the mean number of earthquakes per year producing a shaking of exactly im; the minus sign is required by the negative slope of the hazard curve.

As previously introduced, λ_{im} is commonly computed via the PSHA integral as:

$$\lambda_{im} = \sum_{i=1}^{n_{SZ}} \nu_{m_{min,i}} \int_{m_{min,i}}^{m_{max,i}} \int_{r_{min,i}}^{r_{max,i}} P[IM > im|m, r] f_{M_i}(m) f_{R_i}(r) dm dr \tag{3}$$

where $\nu_{m_{min,i}}$ is the rate of occurrence of earthquakes greater than a suitable minimum magnitude $m_{min,i}$ of the i^{th} seismogenic zone (SZ), $f_{M_i}(m)$ is the magnitude distribution for the i^{th} SZ and $f_{R_i}(r)$ is the distribution of the source i^{th}-to-site distance. Finally, $P[IM > im|m, r]$ represents the probability to exceed im, for a given combination of magnitude m and distance r, whose distribution parameters are usually provided by a suitable assumed Ground Motion Prediction Equation (GMPE).

For the Italian territory, the seismic hazard map is provided by the National Institute of Geology and Vulcanology (INGV) [39]. The map is based on a 5-km span grid and, for each node, seismic hazard data are

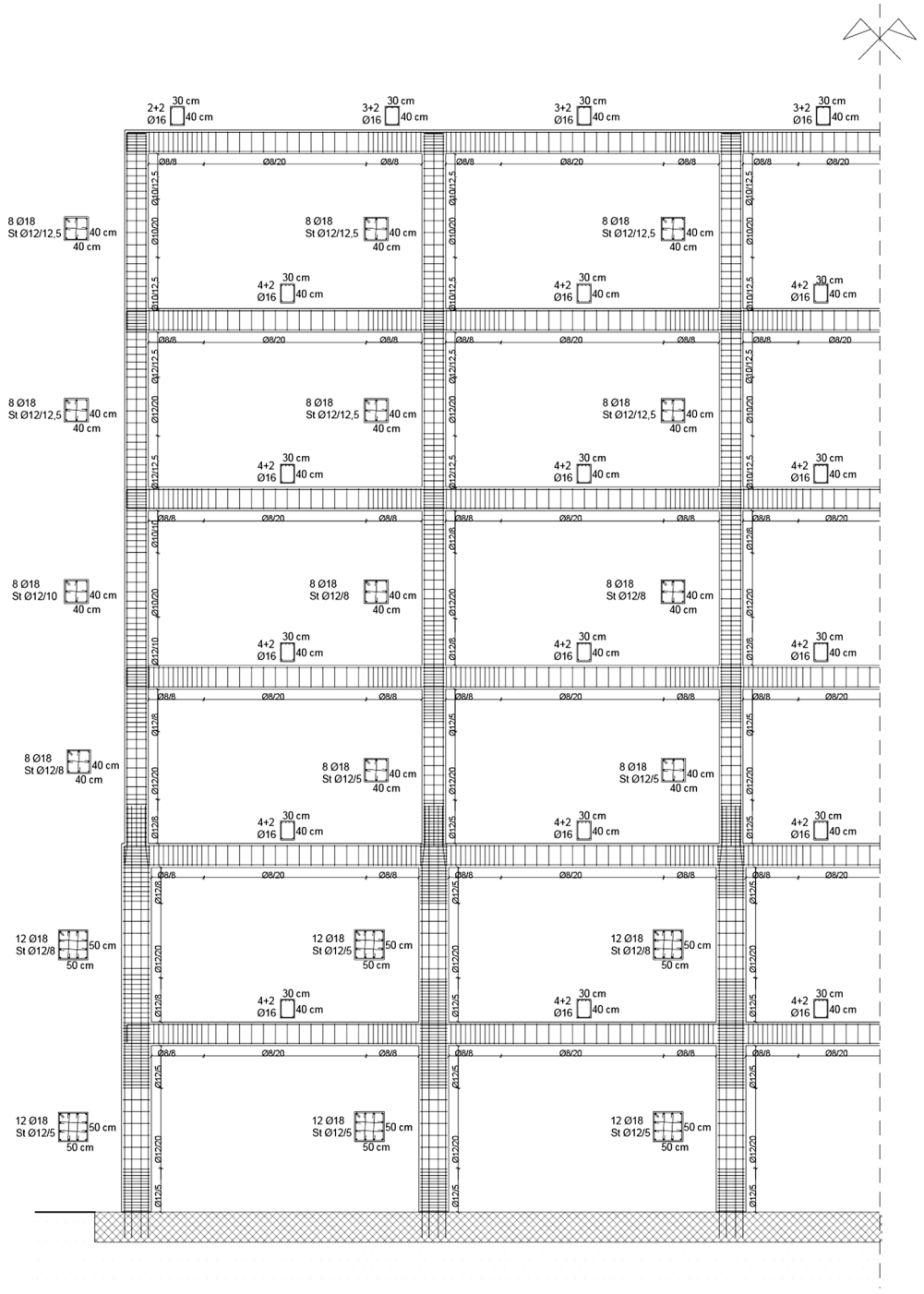

Fig. 7. 6-story RC frame archetype: reinforcement arrangement.

provided, with reference to nine return times, that correspond to exceedance probabilities of 2, 5, 10, 22, 30, 39, 50, 63 and 81% in 50 years, respectively. More in detail, the map provides the values of the 16th, 50th and 84th percentile, which consider the epistemic uncertainties involved in the analysis of seismic hazard. Though, to compute the failure rate λ_f, it is necessary to have a continuous hazard function. For this, in the common practical engineering applications, instead of developing a full PSHA, it is also possible to fit those median values (i.e., the 50th percentile) with a quadratic function in the logarithmic space as:

$$\lambda(s) = k_0 e^{(-k_1 \ln(s) - k_2 ln^2(s))} \tag{4}$$

considering only the decreasing branch of the interpolated curve is considered for the further computation of the mean failure rate. In addition, since hazard code estimates are related to 16th, 50th and 84th percentile, it is more suitable to refer to a mean hazard curve instead in assessing seismic reliability. Hence, starting from the median hazard curve, it is possible to derive the mean one with the following equation:

$$\tilde{\lambda}(s) = \lambda(s) e^{(\frac{1}{2}\beta_H^2)} \tag{5}$$

where β_H can be estimated as:

$$\beta_H = \frac{\ln(S_{84\%}) - \ln(S_{16\%})}{2} \tag{6}$$

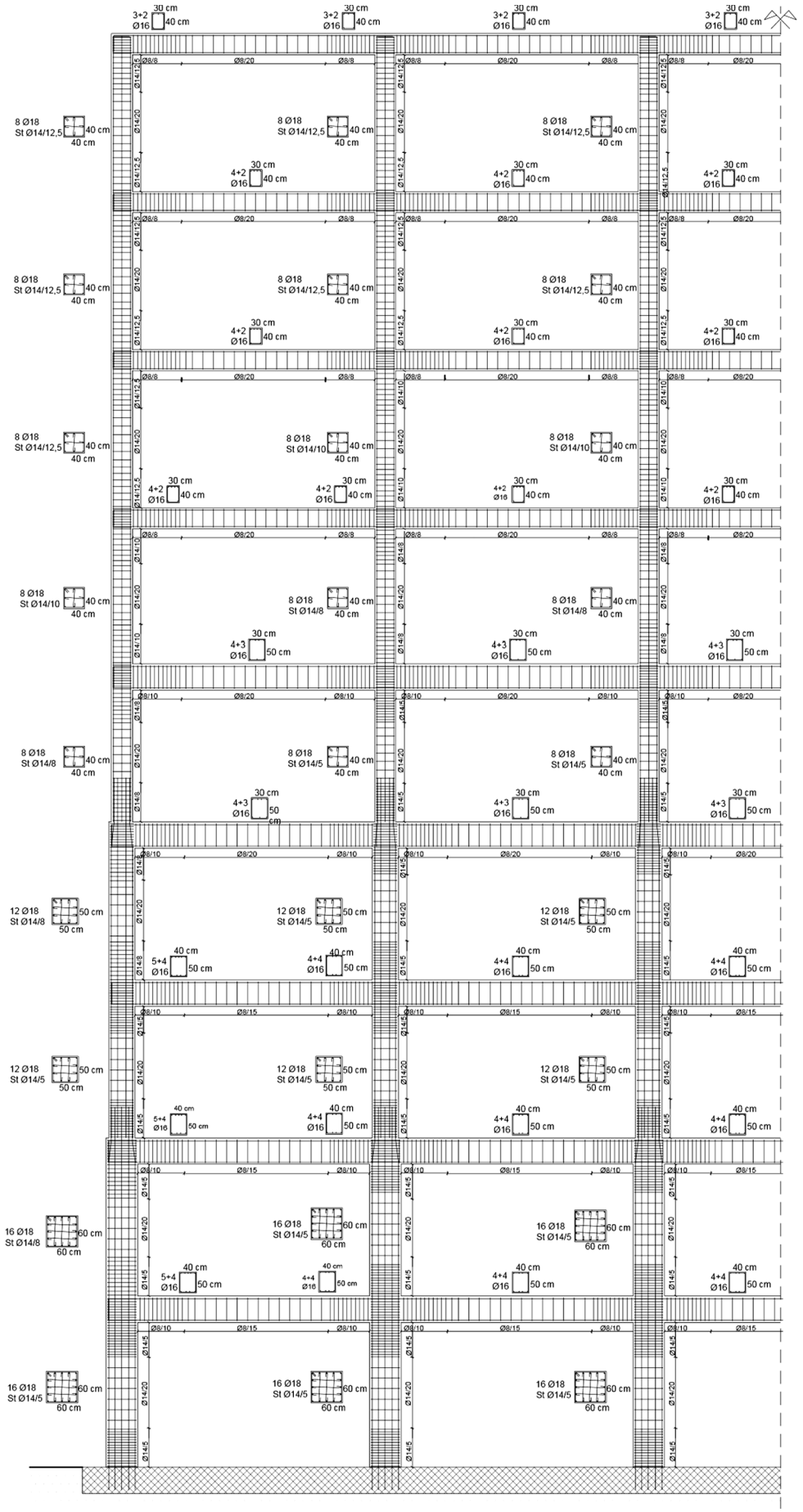

Fig. 8. 9-story RC frame archetype: reinforcement arrangement.

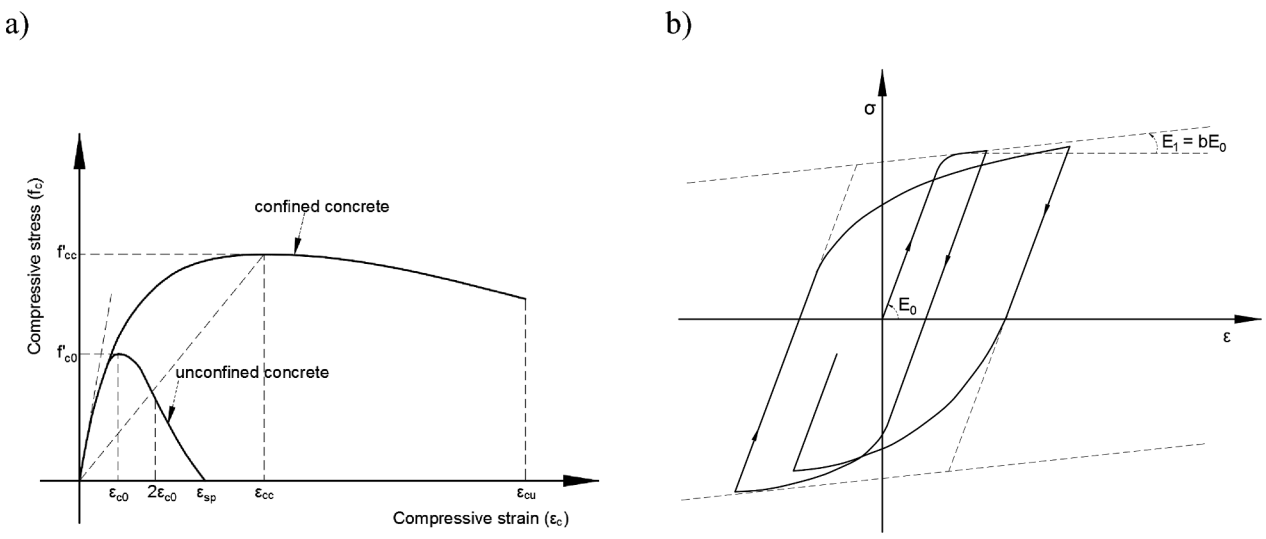

Fig. 9. Adopted constitutive laws: Mander et al. [44] concrete model (a) and Menegotto and Pinto [45] steel model (b).

Table 5
Selected 3-D earthquake records.

Record ID	Event	Date	M_w	R [km]	PGA_H [g]	PGA_Z [g]
1	L'Aquila	06/04/2009	6.1	5.0	0.448	0.443
2	L'Aquila	06/04/2009	6.1	5.1	0.491	0.240
3	Friuli	17/06/1976	5.2	14.3	0.090	0.008
4	Friuli	11/09/1976	5.6	18.6	0.239	0.090
5	Southern Italy	16/01/1981	5.2	21.7	0.109	0.022
6	Umbria-Marche	14/10/1997	5.6	40.7	0.044	0.015
7	Northern Italy	07/06/1980	4.6	11.3	0.060	0.037
8	Southern Italy	09/09/1998	5.6	38.7	0.043	0.017
9	Ancona	21/06/1972	4.0	25.9	0.430	0.121
10	Ancona	14/06/1972	4.7	7.7	0.565	0.275
11	Duzce	12/11/1999	7.3	27.4	1.030	0.323
12	Central Italy	26/10/2016	5.4	3.7	0.757	0.304
13	Western Caucasus	03/05/1991	5.6	17.8	0.563	0.103
14	Pyrgos	26/03/1993	5.4	1.3	0.469	0.076
15	Southern Greece	15/09/1986	4.8	14.3	0.335	0.124
16	Greece	08/11/2014	5.1	9.2	0.403	0.089
17	Greece	24/04/1988	4.2	16.4	0.280	0.039
18	Austria	06/05/1998	4.3	8.0	0.311	0.096
19	Greece	19/05/1995	5.1	15.1	0.284	0.122
20	Greece	14/07/1993	5.6	4.9	0.410	0.127
21	Azores Islands	09/07/1998	6.2	13.3	0.433	0.304
22	Greece	07/09/1999	5.9	26.3	0.158	0.080
23	Central Italy	26/10/2016	5.9	33.9	0.183	0.071
24	Albania	13/06/1993	5.3	58.5	0.148	0.035
25	Central Italy	26/01/2003	4.7	7.9	0.130	0.066
26	Southern Greece	25/10/1984	5.0	15.6	0.193	0.087
27	Friuli	11/09/1976	5.2	6.1	0.201	0.077
28	Norcia	19/09/1979	5.8	40.4	0.085	0.016
29	Ancona	14/06/1972	4.2	9.3	0.433	0.157
30	Gibraltar	04/01/1994	4.9	24.4	0.062	0.045

4.2. Seismic fragility analysis

In Eq. (1), $P[f|im]$ represents the probability to reach and exceed a given damage state level (*failure*), conditioned on a specific ground motion intensity measure $IM = im$. This fragility function is strictly connected with the analyzed structure, and its calibration is commonly based on results carried out with a set of NLTHAs. Several theoretical models and procedures have been proposed in literature for the calibration of $P[f|im]$ parameters; among all, the most used are the Incremental Dynamic Analysis [40], the Cloud-Analysis [41], and the Multi-Stripes Analysis [42].

Regarding the Cloud Analysis approach - that is the most computationally friendly approach - similar considerations on the model parameters can be done: in particular, a fragility curve takes origin from a sample of n ground motions intensities $[im_1, im_2, ...,im_n]$ and the corresponding sample of structural responses $[edp_1, edp_2, ...,edp_n]$. Compared to the IDA method, the Cloud Analysis approach is less time consuming, since the investigated structure is subject to a limited set of n unscaled ground motions records. In this case, the fragility function assumes the following form [44]:

$$P[f|im] = P[EDP > \overline{edp}|im] = 1 - P[EDP \leq \overline{edp}|im] = 1 - \Phi\left[\frac{ln(\overline{edp}) - ln(edp)}{\beta}\right] \quad (7)$$

In Eq. (7), $\overline{edp}$ is the median threshold value of the assumed structural limit state, and edp represents the median estimate of the demand that can be computed with a ln-linear regression model, as:

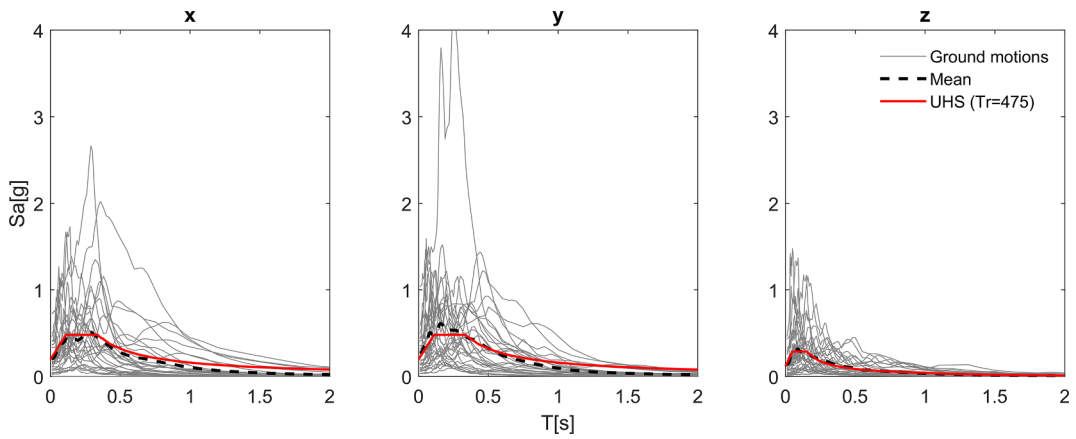

Fig. 10. Selected seismic records: X- (a), Y- (b) and Z- (c) direction.

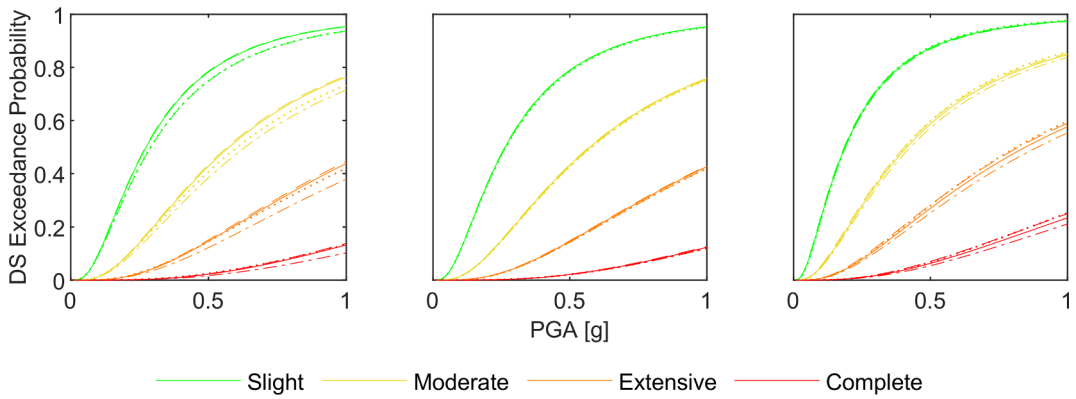

Fig. 11. Slight, Moderate, Extensive and Complete DS fragility curves for 3- (a), 6- (b) and 9- (c) story RC frame archetypes (Solid - reference material (C25/30); Dotted - EAF-C1; Dashed - EAF-C2; Dash-dot – EAF-A).

Table 6
3-Story building fragility parameters.

Concrete Mix	DS1 – Slight		DS2 – Moderate		DS3 – Extensive		DS4 – Complete	
	μ	σ	μ	σ	μ	σ	μ	σ
C25/30	0.274	0.771	0.575	0.771	1.127	0.771	2.364	0.771
EAF-C1	0.29	0.809	0.605	0.809	1.177	0.809	2.454	0.809
EAF-C2	0.272	0.771	0.569	0.771	1.109	0.771	2.318	0.771
EAF-A	0.2915	0.807	0.634	0.807	1.281	0.807	2.785	0.807

Table 7
6-Story building fragility parameters.

Concrete Mix	DS1 – Slight		DS2 – Moderate		DS3 – Extensive		DS4 – Complete	
	μ	σ	μ	σ	μ	σ	μ	σ
C25/30	0.264	0.796	0.573	0.796	1.159	0.796	2.518	0.796
EAF-C1	0.267	0.800	0.581	0.800	1.176	0.800	2.559	0.800
EAF-C2	0.263	0.799	0.571	0.799	1.153	0.799	2.503	0.799
EAF-A	0.265	0.797	0.578	0.797	1.173	0.797	2.561	0.797

$$ln(edp) = a + b \cdot ln(im) \quad (8)$$

Finally, β is the standard deviation of the demand conditioned on im and can be estimated from the regression of the seismic demands as:

$$\beta = \sqrt{\frac{\sum_{i=i}^{n} [ln(edp_i) - (a + b \cdot ln(im_i))]^2}{n - 2}} \quad (9)$$

5. Seismic reliability assessment of the analyzed EAF RC frame archetypes

5.1. Modelling strategy

When dealing with NLTHAs, material non-linearities can be represented implementing lumped or diffused plasticity models [43]. Diffused plasticity models were herein assumed, via the use of fiber-

Table 8
9-Story building fragility parameters.

Concrete Mix	DS1 – Slight		DS2 – Moderate		DS3 – Extensive		DS4 – Complete	
	μ	σ	μ	σ	μ	μ	σ	μ
C25/30	0.188	0.860	0.414	0.860	0.847	0.860	1.866	0.860
EAF-C1	0.189	0.839	0.407	0.839	0.815	0.839	1.753	0.839
EAF-C2	0.186	0.865	0.405	0.865	0.822	0.865	1.794	0.865
EAF-A	0.190	0.865	0.427	0.865	0.891	0.865	2.005	0.865

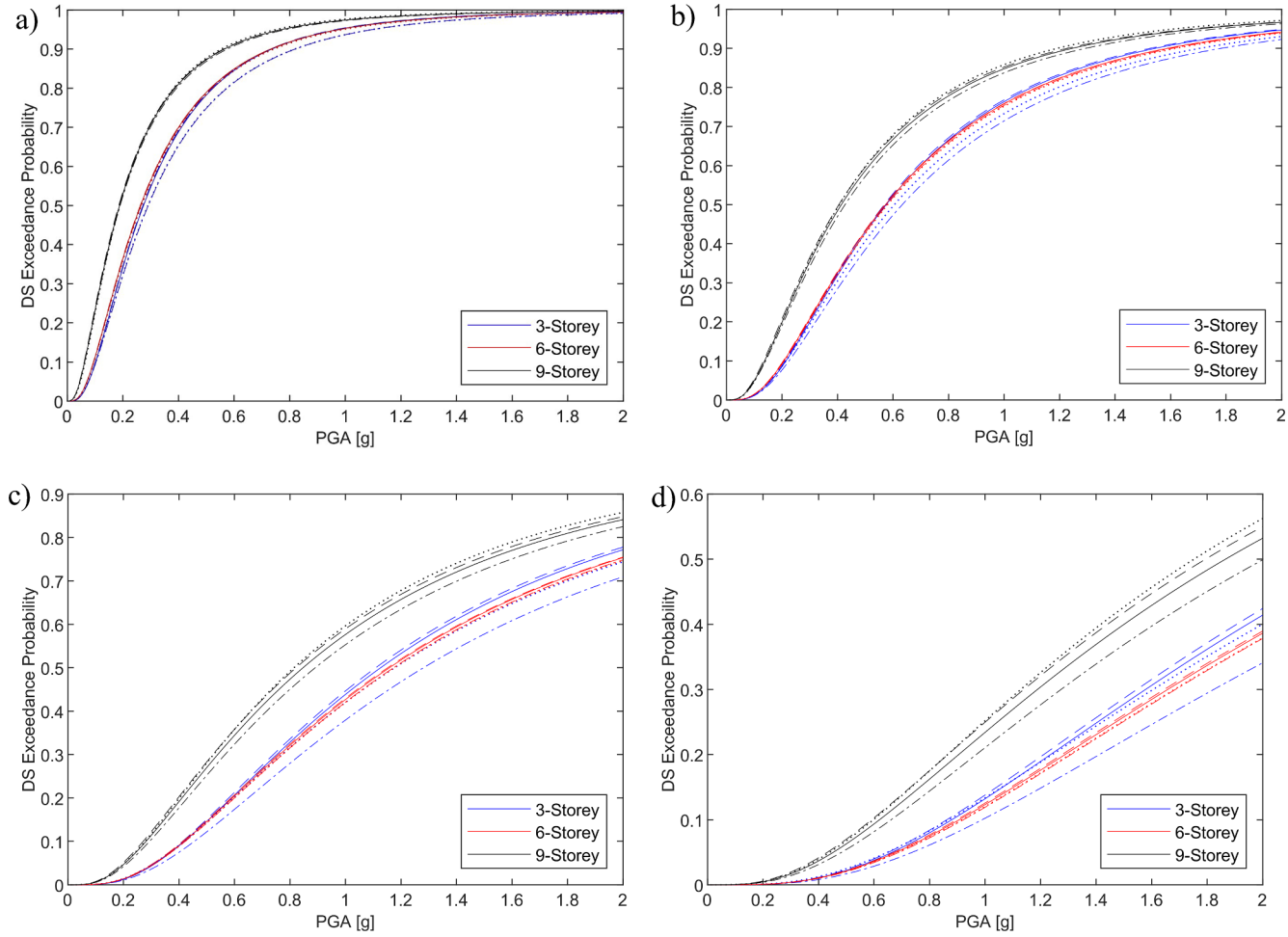

Fig. 12. Comparison between fragilities derived for the 3-, 6- and 9 story RC frame archetypes: Slight (a), Moderate (b), Extensive (c) and Complete (d) DSs.

section discretization technique. Here, the Mander et al. [44] model was assumed for both unconfined and confined concrete materials whereas the Menegotto-Pinto [45] steel model was used to characterize non-linear behavior of reinforcing bars. Even if few cyclic tests on EAF concrete specimens can be currently retrieved in literature [30,31], it was reasonably to assume the adoption of Mander et al. [44] constitutive model for EAF concrete too, given the similar behavior under monotonic uniaxial compressive test to ordinary mixes. Fig. 9 shows the adopted material constitutive laws, with concrete parameters were defined according to those listed in Table 4.

Reference concrete material is the C25/30 strength class from the Italian Building Code [5], while the EAF concrete characteristics are obtained through the ratio coefficients listed in Table 3. Reinforcement bars material characteristics are defined by a mean yield strength of 483 MPa, elasticity modulus of 200 GPa and a hardening parameter of 0.5%, that conform to a B450C steel type according to [5].

RC frames were modelled with non-linear frame elements characterized by 5 integration points, constrained with fixed nodes at the base, and, in addition, rigid diaphragms were inserted in order to properly characterize rigid axial floor behavior. A 5% Rayleigh damping factor is considered, using the Hilber - Hughes – Taylor integration scheme for the execution of the subsequent NLTHAs.

5.2. Seismic record selection

NLTHAs were then carried out with SeismoStruct software [46]. Fragility analysis based on the Cloud Analysis approach is defined deriving for each NLTHA a data point linking two parameters, an Intensity Measure (IM) representative of a generic seismic record and a structural response parameter, i.e. the Engineering Demand Parameter (EDP). Different intensity or response parameters can be considered for the construction of fragility curves. Among possible IMs, peak ground acceleration (PGA) and spectral acceleration (Sa) are the two main parameters used in this kind of studies. The EDP parameters generally

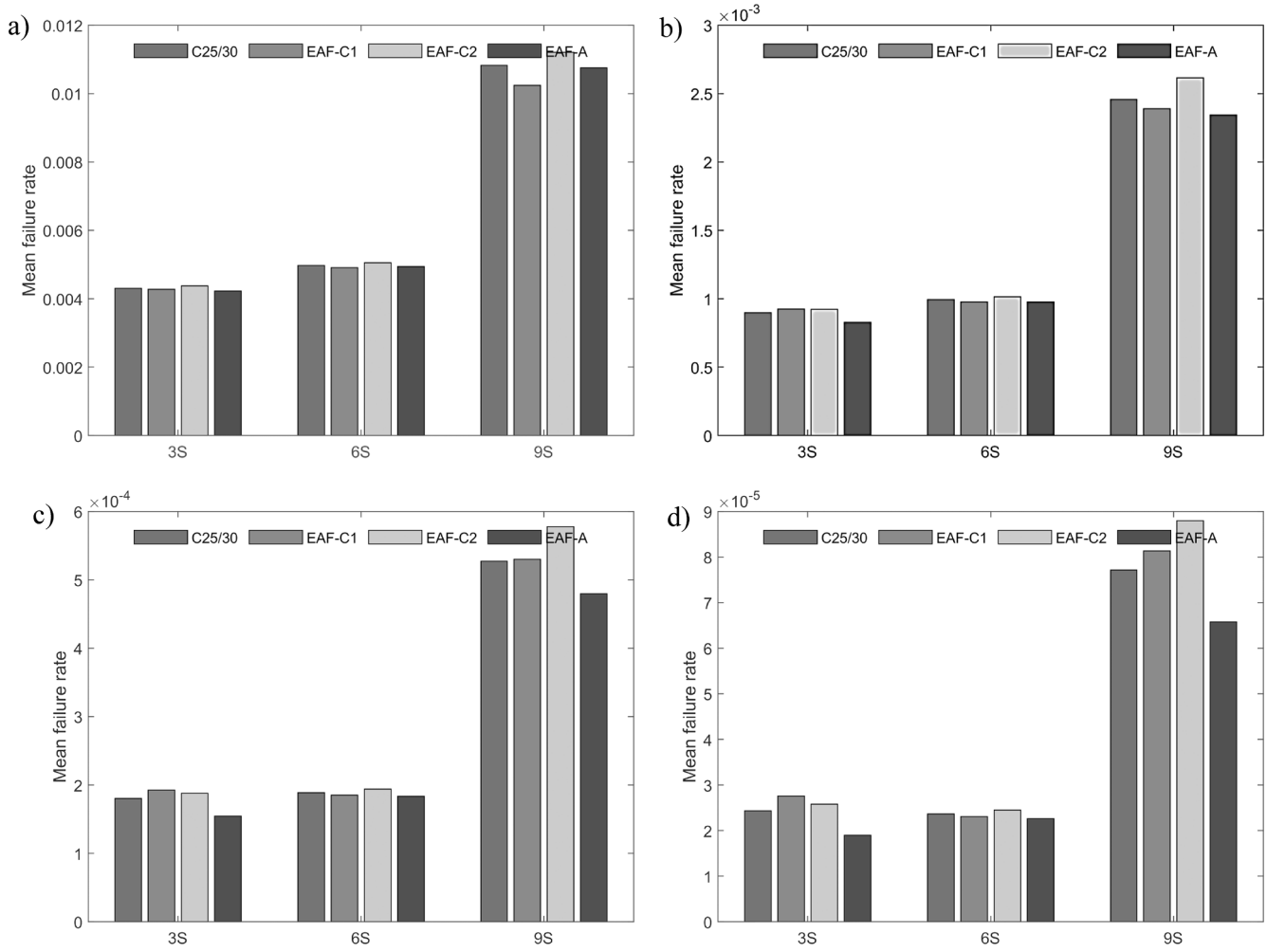

Fig. 13. Comparison between mean failure rates derived for 3-, 6- and 9-story RC frame archetypes: Slight (a), Moderate (b), Extensive (c) and Complete (d) DSs.

vary more and may depend also on the type of structure that is being analyzed. EDP parameters have been a matter of studies since the Performance Based Earthquake Engineering was introduced. Whittaker et al. [47] studied the EDP for structural framing systems, Ghobarah [48] studied drift limits as EDP parameters associated with damage levels, while lately Stocchi and Richard [49] studied the sensitivity of different engineering demand parameters based on structure typology and assessment method. In this paper, the maximum interstory drift ratio (IDR) is the chosen EDP. Even though IDR is a global parameter, it permits to capture eventual local damage (e.g. soft stories). In this study, four damage states (DSs) were considered: Slight, Moderate, Extensive and Complete. For the definition of the associated IDR limits, static non-linear analyses (pushover) were conducted, and the limits were derived with values equal to 0.4%, 0.8%, 1.5% and 3%, respectively. These limits are similar to those proposed by Ghobarah [48] for ductile RC moment frame structures. Hazus MH 2.1 Technical Manual [50] for Earthquake Loss Estimation Methodology proposes a reduction factor for mid-rise and high-rise buildings, respectively 2/3 and 1/2, to account for higher mode effects and eventual differences between average and individual inter-story drift. This recommendation was also taken into account in the present study.

6. Results and discussion

A total of twelve different models, created from the combination of three different geometrical configurations and four different materials, were analyzed with NLTHAs, adopting for each case the same set of 30 ground motion records listed in Table 5. Seismic records were used considering all their three main components: Fig. 10 shows respectively horizontal X-, Y-, and vertical spectral response for each of the records considered, highlighting how the computed mean spectrum of the considered records well approximates the 475-years uniform hazard spectrum (UHS) for the analyzed site. The buildings performance was then evaluated with respect to four DSs varying from Slight to Complete.

From the time histories registered building responses, fragility curves were built for each case, in accordance with the Cloud Analysis method described in Section 4.2. Fig. 11 shows fragility curves for Slight, Moderate, Extensive and Complete damage in green, yellow, orange and red color respectively. Additionally, solid lines were used for frames realized with the reference concrete; instead, dotted, dashed and dash-dot lines were used for EAF-C1, EAF-C2 and EAF-A concretes, respectively. Tables 6–8 list the fragility parameters, namely the mean and standard deviation for each concrete class and DS, of the analyzed building configurations (3-, 6- and 9-story).

Results show how EAF concrete building performance to seismic solicitation is very similar to that of the buildings made with the reference material. For the 3- and 9-story buildings the fragility curves (Fig. 11a and c) tend to vary more while considering superior DSs, with the EAF-A material less vulnerable to seismic actions. The 6-story building has almost an identical response for all the materials considered. In fact, the fragility curves (Fig. 11b) are almost overlapping for all kind of materials used. Tables 6–8 lists main fragility curves parameters derived for all the twelve investigated RC frame archetypes.

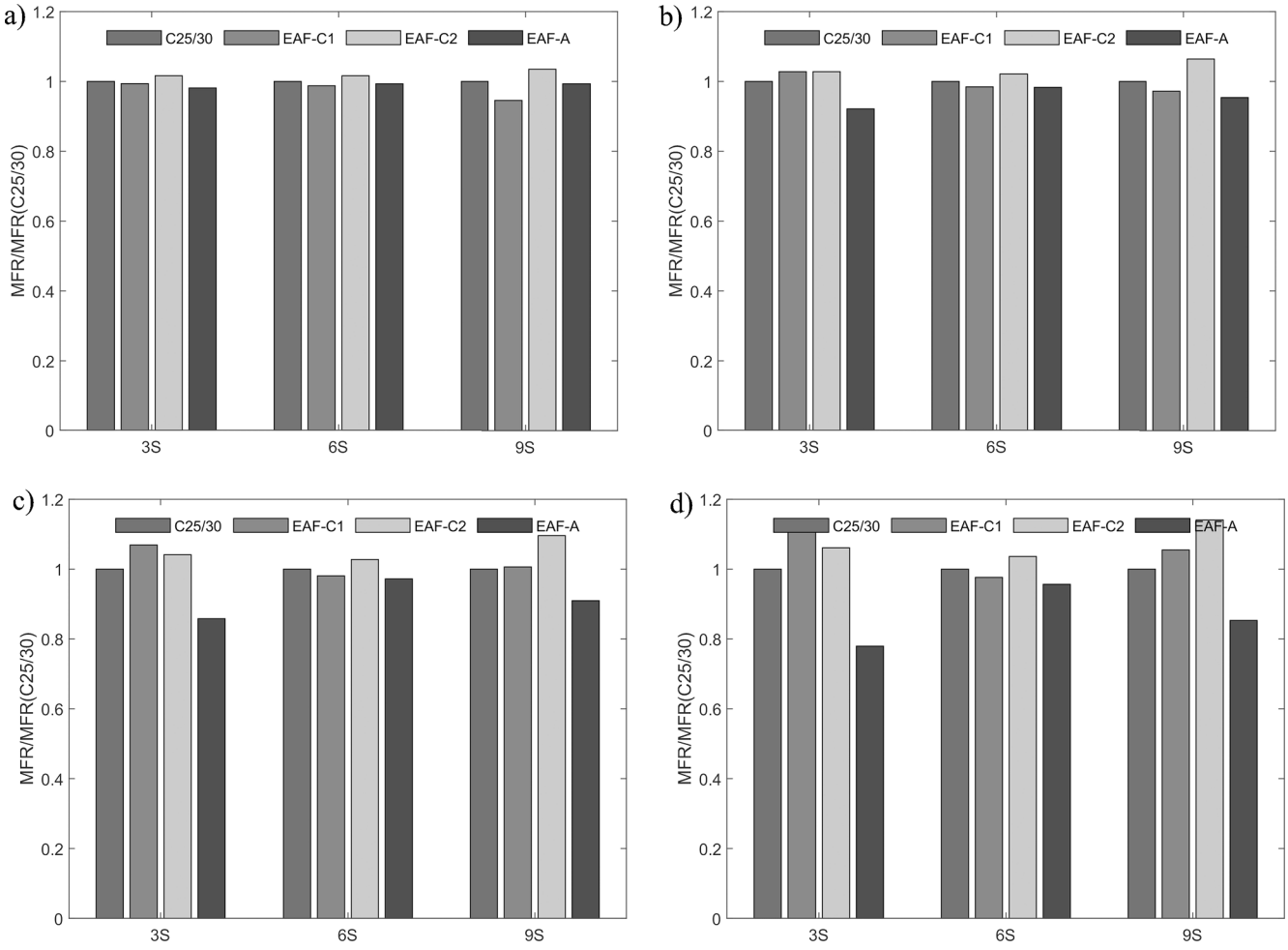

Fig. 14. Ratios between EAF concrete and reference material mean failure rates: Slight (a), Moderate (b), Extensive (c) and Complete (d) DSs.

Table 9
Concrete volume estimated for the construction of the buildings.

	Column [m^3]	Beam [m^3]	Slab [m^3]	Total [m^3]
3-Story	33.0	38.0	225	296
6-Story	78.5	75.5	450	604
9-Story	139.5	155.5	675	970

Results show how EAF concrete building performance to seismic solicitation is very similar to that of the buildings made with the reference material. Fig. 11 highlights how for the 3- and 9-story buildings the fragility curves tend to vary more while considering superior DSs, with the EAF-A material less vulnerable to seismic actions, whereas the 6-story building has almost an identical response for all the materials considered. From one side, among the EAF mixes, results show how the EAF-A archetypes seem to have a slightly better seismic response. This is mainly due to similar mechanical characteristics - in particular, in terms of stiffness - with respect to reference concrete, but at the same time, it is characterized by higher weight, thus resulting in increased fundamental periods and, consequently, slightly lower drift profiles. From the other side, looking at the three different archetypes, the changes in mass and stiffness seem to balance their impact on the overall structural response for the intermediate case (i.e., 6-story building). This is correlated also to the fact that the fundamental periods of this archetype are quite long, thus implying low spectral accelerations characterized by low variability, with higher modes that are not yet impacting the results like in the 9-story case. Tables 6–8 lists main fragility curves' parameters derived for all the twelve investigated RC frame archetypes.

Comparing the models which differ in height, the 9-story-one results more vulnerable than the 3- and 6-story cases, and this can be seen also in the fragility curves in Fig. 12, regardless of the considered DS.

Hence, mean failure rates were computed for each DS and RC frame archetype: Fig. 13 shows the final results classified with reference to each considered DS. Mean failure rates are characterized by a decreasing trend of one order of magnitude moving from less severe to stronger DSs, with values in the order of 10^{-2} for Slight DS, 10^{-3} for Moderate DS, 10^{-4} for Extensive DS and 10^{-5} for Complete DS. Mean failure rates computed for the EAF buildings are almost similar to the values obtained for the ones assessed considering reference C25/30 concretes, thus confirming again the achievement of similar safety margins against horizontal actions induced by earthquakes of buildings designed as made with ordinary concretes but realized with partial of full replacement of NAs with EAF aggregates.

It can also be observed how mean failure fate values computed for the 9-story RC frame archetype are almost twice the ones derived for the 3- and 6- story archetypes, and this regardless the type of concrete. This fact underlies how it seems that the adoption of current code recommendations does not allow to design buildings characterized by the same level of seismic reliability, but some differences can be observed as herein shown, in particular comparing low-to-medium rise buildings with higher ones.

Fig. 14 shows the ratios between mean failure rates obtained for the EAF RC frame archetypes and those computed for their respective benchmark configurations (i.e. with NA concrete), highlighting how the

partial or full replacement of NAs with EAF aggregates has a low impact in terms of seismic reliability levels with the investigated structural systems are subject to seismic events.

From an environmental sustainability point of view, it is worth recalling that if the three considered buildings were to be built, nearly more than 2000 m^3 of concrete would have to be used (Table 9), thus using recycled materials may reduce sensibly the ecological footprint of these constructions.

In terms of natural aggregates consumption, such volume means that about 3400 tons of NA could be saved if EAF slag fully substitutes the virgin material. Such estimation has been performed considering about 1700 kg of NA/m^3 in a mix design for a reference concrete.

7. Conclusion

Recent scientific literature showed how EAF concretes are characterized by a good bearing capacity under static loads, offering often better strength than NA concrete. However, when replacing NAs with EAF aggregates, concrete is characterized by an increased self-weight, and this issue can impact on the structural response of EAF buildings do to the intrinsic variation of weight (mass) and elastic modulus (stiffness), that can affect directly the building performance as they may change the eigen values of the structure. The present paper had therefore as main aim to investigate in detail such issue, demonstrating how the use of EAF aggregates in replacement of NAs in code-conforming structural systems, can ensure a similar seismic reliability level. In particular, different RC-frame archetypes with 3-, 6- and 9- stories were first designed as made with ordinary C25/30 concretes accordingly to the new Italian Building Code issued in 2018 for a site located in medium-to-high seismicity in the municipality of Pordenone, northeastern Italy. Hence, a seismic reliability assessment was carried out considering the designed structural systems realized with different concrete mixes characterized by the partial and full replacement of NAs with EAF aggregates. Mean failure rates were computed for each combination of RC archetype and concrete mix on the basis of the seismic fragility curves derived with the Cloud Analysis method performing a set of 30 NLTHAs with 3-D seismic records and referring to four different DSs. On the basis of the results herein presented, the following concluding remarks can be outlined:

- this study demonstrates that even when using materials with definitely better properties than the reference one (like in terms of concrete strength for the EAF concretes), the overall response of the structure might be not improved, and this is mainly due to the change of other parameters like self-weight and elastic moduli. The same applies for materials with apparently poorer properties, such as in the case of EAF-A concrete, which is characterized by a relatively lower compressive strength and higher specific weight than the reference mix;
- the resulting seismic reliability estimates for the designed code-conforming RC frame archetypes made with EAF concretes is comparable with that of the same structural systems made with ordinary concretes;
- resulting mean failure rates are similar for 3- and 6- RC frame archetypes for each investigated DS, whereas a significant variation was observed with respect to the 9-story case study, where the outcomes are almost twice times higher, thus highlighting how for higher buildings current design approaches may not ensure the same seismic reliability level with respect to that of low-to-medium high ones.

Future developments of the present study will focus in further investigating the ability of design practices illustrated in the current Italian Building Code [5] in ensuring uniform seismic reliability levels over the entire Italian peninsula, as well as the analysis of seismic reliability of other RC archetypes realized with different sustainable concretes, like foamed ones, that are characterized by different ratios of self-weight over strength [51].

References

[1] United Nations (2015) Resolution adopted by the General Assembly on 25 September 2015. 70/1. Transforming our world: the 2030 Agenda for Sustainable Development.

[2] European Aggregates Association (2017) Annual Review 2016-2017. [available online at: http://www.uepg.eu/uploads/Modules/Publications/uepg-ar2016-17_32pages_v10_18122017_pbp_ small.PDF].

[3] FHWA (1997) User Guidelines for Waste and Byproduct Materials in Pavement Construction. Federal Highway Administration Research and Technology Report no. FHWA-RD-97-148.

[4] EN 12620 (2008) Aggregates for concrete. Comité Européen de Normalisation, Brussels, Belgium.

[5] DM 17/01/2018 (2018) Aggiornamento delle Norme Tecniche per le Costruzioni, Roma, Italy. [in Italian].

[6] Saikia N, de Brito J. Use of plastic waste as aggregate in cement mortar and concrete preparation: A review. Constr Build Mater 2012;34:385–401. https://doi.org/10.1016/j.conbuildmat.2012.02.066.

[7] Aldahdooh MAA, Jamrah A, Alnuaimi A, Martini MI, Ahmed MSR, Ahmed ASR. Influence of various plastics-waste aggregates on properties of normal concrete. J Build Eng 2018;17:13–22. https://doi.org/10.1016/j.jobe.2018.01.014.

[8] Jin W, Meyer C, Baxter S. "Glascrete" – Concrete with Glass Aggregate. ACI Mater J 2000;97(2):208–13.

[9] Ramdani S, Guettala A, Benmalek ML, Aguiar JB. Physical and mechanical performance of concrete made with waste rubber aggregate, glass powder and silica sand powder. J Build Eng 2019;21:302–11. https://doi.org/10.1016/j.jobe.2018.11.003.

[10] Fernández-Ruiz MA, Gil-Martín LM, Carbonell-Márquez JF, Hernández-Montes E. Epoxy resin and ground tyre rubber replacement for cement in concrete: Compressive behaviour and durability properties. Constr Build Mater 2018;173:49–57. https://doi.org/10.1016/j.conbuildmat.2018.04.004.

[11] Alsaif A, Bernal SA, Guadagnini M, Pilakoutas K. Freeze-thaw resistance of steel fibre reinforced rubberised concrete. Constr Buil Mater 2019;195:450–8. https://doi.org/10.1016/j.conbuildmat.2018.11.103.

[12] Cardoso C, Camões A, Eires R, Mota A, Araújo J, Castro F, Carvalho J. Using foundry slag of ferrous metals as fine aggregate for concrete. Res Conserv Recycl 2018;138:130–41. https://doi.org/10.1016/j.resconrec.2018.05.020.

[13] Parron-Rubio ME, Perez-García F, Gonzalez-Herrera A, Rubio-Cintas MD. Concrete properties comparison when substituting a 25% cement with slag from different provenances. Materials 2018;11(6):1029. https://doi.org/10.3390/ma11061029.

[14] García-Cuadrado J, Santamaría-Vicario I, Rodríguez A, Calderón V, Gutiérrez-González S. Lime-cement mortars designed with steelmaking slags as aggregates and validation study of their properties using mathematical models. Constr Build Mater 2018;188:210–20. https://doi.org/10.1016/j.conbuildmat.2018.08.093.

[15] Skaf M, Ortega-López V, Fuente-Alonso JA, Santamaría A, Manso JM. Ladle furnace slag in asphalt mixes. Constr Build Mater 2016;122:488–95. https://doi.org/10.1016/j.conbuildmat.2016.06.085.

[16] Pellegrino C, Gaddo V. Mechanical and durability characteristics of concrete containing EAF slag as aggregate. Cem Concr Compos 2009;31(9):663–71. https://doi.org/10.1016/j.cemconcomp.2009.05.006.

[17] Arribas I, Santamaría A, Ruiz E, Ortega-López V, Manso JM. Electric arc furnace slag and its use in hydraulic concrete. Constr Build Mater 2015;90:68–79. https://doi.org/10.1016/j.conbuildmat.2015.05.003.

[18] Rondi L, Bregoli G, Sorlini S, Cominoli L, Collivignarelli C, Plizzari G. Concrete with EAF steel slag as aggregate: A comprehensive technical and environmental characterisation. Compos Part B 2016;90:195–202. https://doi.org/10.1016/j.compositesb.2015.12.022.

[19] Liapis A, Anastasiou EK, Papachristoforou M, Papayianni I. Feasibility Study and Criteria for EAF Slag Utilization in Concrete Products. J Sustain Metall 2018;4(1):68–76. https://doi.org/10.1007/s40831-017-0152-2.

[20] Qasrawi H. The use of steel slag aggregate to enhance the mechanical properties of recycled aggregate concrete and retain the environment. Constr Build Mater 2014;54:298–304. https://doi.org/10.1016/j.conbuildmat.2013.12.063.

[21] Faleschini F, Alejandro Fernández-Ruíz M, Zanini MA, Brunelli K, Pellegrino C, Hernández-Montes E. High performance concrete with electric arc furnace slag as aggregate: mechanical and durability properties. Constr Build Mater 2015;101:113–21. https://doi.org/10.1016/j.conbuildmat.2015.10.022.

[22] Pellegrino C, Cavagnis P, Faleschini F, Brunelli K. Properties of concretes with black/oxidizing electric arc furnace slag aggregate. Cem Concr Compos 2012;37:232–40. https://doi.org/10.1016/j.cemconcomp.2012.09.001.

[23] Ortega-López V, Fuente-Alonso JA, Santamaría A, San-José JT, Aragón Á. Durability studies on fiber-reinforced EAF slag concrete for pavements. Constr Build Mater 2018;163:471–81. https://doi.org/10.1016/j.conbuildmat.2017.12.121.

[24] Santamaría A, Orbe A, Losañez MM, Skaf M, Ortega-López V, González JJ. Self-compacting concrete incorporating electric arc-furnace steelmaking slag as aggregate. Mater Des 2017;115:179–93. https://doi.org/10.1016/j.matdes.2016.11.048.

[25] Qasrawi H. Fresh properties of green SCC made with recycled steel slag coarse aggregate under normal and hot weather. J Clean Prod 2018;204:980–91. https://doi.org/10.1016/j.jclepro.2018.09.075.

[26] Pellegrino C, Faleschini F. Experimental behavior of reinforced concrete beams with electric arc furnace slag as recycled aggregate. ACI Mater. J. 2013;110:197–206.

[27] De Domenico D, Faleschini F, Pellegrino C, Ricciardi G. Structural behavior of RC beams containing EAF slag as recycled aggregate: Numerical versus experimental results. Constr Build Mater 2018;171:321–37. https://doi.org/10.1016/j.conbuildmat.2018.03.128.
[28] Faleschini F, Santamaria A, Zanini MA, San José J-T, Pellegrino C. Bond between steel reinforcement bars and Electric Arc Furnace slag concrete. Mater Struct 2017;50:170. https://doi.org/10.1617/s11527-017-1038-2.
[29] Lee J-M, Lee Y-J, Jung Y-J, Park J-H, Lee B-S, Kim K-H. Ductile capacity of reinforced concrete columns with electric arc furnace oxidizing slag aggregate. Constr Build Mater 2018;162:781–93. https://doi.org/10.1016/j.conbuildmat.2017.12.045.
[30] Faleschini F, Hofer L, Zanini MA, Dalla Benetta M, Pellegrino C. Experimental behavior of beam-column joints made with EAF concrete under cyclic loading. Eng Struct 2017;139:81–95. https://doi.org/10.1016/j.engstruct.2017.02.038.
[31] Faleschini F, Bragolusi P, Zanini MA, Zampieri P, Pellegrino C. Experimental and numerical investigation on the cyclic behavior of RC beam column joints with EAF slag concrete. Eng Struct 2017;152:335–47. https://doi.org/10.1016/j.engstruct.2017.09.022.
[32] Pomaro B, Gramegna F, Cherubini R, De Nadal V, Salomoni V, Faleschini F. Gamma-ray shielding properties of heavyweight concrete with Electric Arc Furnace slag as aggregate: An experimental and numerical study. Constr Build Mater 2019;200:188–97.
[33] Pellegrino C, Faleschini F. Experimental database of EAF slag use in concrete. Sustainability Improvements in the Concrete Industry Switzerland: Springer; 2016. https://doi.org/10.1007/978-3-319-28540-5.
[34] Zanini MA. Structural reliability of bridges realized with reinforced concretes with electric arc furnace slag aggregates. Eng Struct 2019;188:305–19. https://doi.org/10.1016/j.engstruct.2019.02.052.
[35] Santamaria A, Faleschini F, Giacomello G, Brunelli K, San José JT, Pellegrino C, Pasetto M. Dimensional stability of electric arc furnace slag in civil engineering applications. J Clean Prod 2018;205:599–609. https://doi.org/10.1016/j.jclepro.2018.09.122.
[36] Cornell CA, Krawinkler H. Progress and challenges in seismic performance assessment. PEER Centre News 2000;3(2):1–3.
[37] Cornell C. Engineering seismic risk analysis. Bull Seismol Soc Am 1968;58(5):1583–606.
[38] McGuire RK. Probabilistic seismic hazard analysis and design earthquakes: closing the loop. Bull Seismol Soc Am 1995;85(5):1275–84.
[39] INGV. Interactive Seismic Hazard Maps. Available at: http://esse1-gis.mi.ingv.it/s1_en.php [last access 04/03/2019].
[40] Vamvatsikos D, Cornell CA. Applied incremental dynamic analysis. Earthquake Spectra 2004;20(2):523–53. https://doi.org/10.1193/1.1737737.
[41] Jalayer F, Cornell CA. Direct probabilistic seismic analysis: implementing non-linear dynamic assessments. Stanford University; 2003.
[42] Baker JW. Efficient analytical fragility function fitting using dynamic structural analysis. Earthquake Spectra 2015;31(1):579–99. https://doi.org/10.1193/021113EQS025M.
[43] Taucer FF, Spacone E, Filippou FC. A fiber beam-column element for seismic response analysis of reinforced concrete structures. Report No. UCB/EERC-91/17 Earthquake Engineering. Berkeley: Research Center, University of California; 1991.
[44] Mander JB, Priestley MJN, Park R. Theoretical stress-strain model for confined concrete. J Struct Eng 1988;114(8):1804–26.
[45] Menegotto M, Pinto PE. Method of analysis for cyclically loaded reinforced concrete plane frames including changes in geometry and non-elastic behavior of elements under combined normal force and bending. Proc IABSE Symp Resistance Ultimate Deformability Struct Acted by Well Defined Repeated Loads, Int Assoc Bridge Struct Eng, Lisbon, Portugal 1973;13:15–22.
[46] SeismoSoft. SeismoStruct – a computer program for static and dynamic nonlinear analysis of frames structures; 2013. Available at: http://www.seismosoft.com.
[47] Whittaker A, Deierlein GG, Hooper J, Merovich A. Engineering demand parameters for structural framing systems. Task 2.2 report for the ATC-58 project, Applied Technology Council (available from www.ATCouncil.org). Redwood: City, California; 2004.
[48] Ghobarah A. On drift limits associated with different damage levels. International workshop on Performance based design: concepts and implementations, 28 June- 1 July 2004; 2004.
[49] Stocchi A, Richard B. Sensitivity of engineering demand parameters as a function of structural typology and assessment method. Nuclear Eng Des 2019;343:151–65. https://doi.org/10.1016/j.nucengdes.2019.01.006.
[50] FEMA (2012) Earthquake Model, Hazus-MH 2.1 Technical Manual. Federal Emergency Management Agency, Washington DC, US (available at: www.fema.gov/plan/prevent/hazus).
[51] Falliano D, De Domenico D, Ricciardi G, Gugliandolo E. Compressive and flexural strength of fiber-reinforced foamed concrete: Effect of fiber content, curing conditions and dry density. Constr Build Mater 2019;198:479–93. https://doi.org/10.1016/j.conbuildmat.2018.11.197.